PAPER

Check for updates

Ethanolamine-assisted low-temperature crystallization of hydroxide nanoparticle ink into transparent and conductive ITO layers

Yujing Liu, [ID] *[a] Thierry Moser,[a] Christian Andres,[a] Lovro Gorjan,[b] Arndt Remhof, [ID][c] Frank Clemens,[b] Thomas Graule,[b] Ayodhya N. Tiwari[a] and Yaroslav E. Romanyuk [ID] *[a]

Low-temperature crystallization is desired for achieving solution processable transparent conductive oxide (TCO) layers. Here we demonstrate a low-temperature crystallization of tin doped indium oxide (ITO) layers by taking preformed indium–tin hydroxide nanoparticles as the precursor and applying surface modification with ethanolamine on the as-prepared layers. Surface modification with ethanolamine is shown to speed up the dehydration of the hydroxide precursor, resulting in earlier onset of crystallization into the cubic bixbyite ITO phase with a larger crystal size. The ethanolamine-modified ITO nanoparticle layer possesses fewer surface hydroxyl groups as compared to the non-treated layer, corresponding to a higher charge carrier concentration, as manifested in a near IR absorption. The nanoparticle ITO layer shows dc conductivity two times higher than that of the non-treated layer. A conductivity of 43 S cm^{-1} combined with a high optical transmittance of above 90% in the 380–1100 nm wavelength range is obtained for the nanoparticle ITO layer annealed at 300 °C.

1. Introduction

Transparent conducting oxides (TCOs) fabricated *via* vacuum sputtering techniques are widely applied as transparent electrodes in flat panel displays, touch panel displays, thin film solar cells and other opto-electronic devices.[1–3] Wet-chemical processed TCOs, as a promising alternative to sputtered TCOs, have attracted a lot of attention due to their compatibility with roll-to-roll printing techniques and potential to be easily scaled up with less material waste.[4–6] By far, the performance of TCO layers fabricated *via* wet-chemical approaches is still inferior to the ones fabricated by sputtering, with a sheet resistance of hundreds to thousands Ω per square.[7–9]

The use of preformed crystalline nanoparticles (NPs) is considered as one strategy towards conductive TCO layers. In the early studies by Ederth *et al.* individual ITO nanoparticles were found to have a resistivity as low as 2×10^{-4} Ω cm on par with sputtered dense ITO films by analysing spectral optical reflectance and transmittance using effective medium theory.[10,11] However, the electrical conductivity of thin films

processed from nanoparticle dispersion was much lower, on the order of 10^{-2} Ω cm after annealing at 800 °C due to separation between the micrometre-sized clusters of nanoparticles. Nanocrystals (NCs) of TCOs can be synthesized by different methods such as non-aqueous sol–gel[12,13] or hot injection.[7] In recent work by Song *et al.*,[7] ITO nanocrystals in a size of 11 ± 2.4 nm were synthesized *via* a hot-injection synthesis and the processed thin film reached a sheet resistance of 112 Ω sq^{-1} with a transparency of 87% after 1 hour UV exposure and a post-treatment at 300 °C for 6 hours in a reducing atmosphere. One limitation of this approach is that a dispersing agent for steric stabilization is required to achieve a stable ink formulation. The use of the dispersing agent creates unwanted gaps between NCs, which impede the electron transport and decrease electrical conductivity. In recent work by Kim *et al.*,[14] the gaps between adjacent nanoparticles were filled with precursors composed of nitrate, and the improvement of carrier mobility in the case of Ce-doped ITO layers was observed. However, the post-deposition annealing temperature was as high as 500 °C.

Using molecular precursors such as metal salts or metal alkoxides is another wet-chemical approach to obtain TCO layers. It was reported that the resistivity of molecular precursor processed ITO films can be as low as 10^{-4} Ω cm, approaching the values of sputtered ITO but a prolonged thermal annealing at 450–600 °C under a controlled atmosphere had to be applied.[15–17] To facilitate the formation of metal oxide and the reduction of crystallization temperature, several strategies were proposed such as the tuning of precursor chemistry and use of chemical assisted annealing.[18] Chemical combustion synthesis,

[a]Laboratory for Thin Films and Photovoltaics, Empa-Swiss Federal Laboratories for Materials Science & Technology, Überlandstrasse 129, Dübendorf, CH-8600, Switzerland. E-mail: Yujing.Liu85@gmail.com; Yaroslav.Romanyuk@empa.ch

[b]Laboratory for High Performance Ceramics, Empa-Swiss Federal Laboratories for Materials Science & Technology, Überlandstrasse 129, Dübendorf, CH-8600, Switzerland

[c]Laboratory for Materials for Energy Conversion, Empa-Swiss Federal Laboratories for Materials Science & Technology, Überlandstrasse 129, Dübendorf, CH-8600, Switzerland

This journal is © The Royal Society of Chemistry 2019

J. Mater. Chem. A, 2019, 7, 3083–3089 | 3083

a method utilizing the exothermic combustion of precursors to provide localized energy supply, was effective in reducing the processing temperature comparing with conventional methods. Following this method, the dc conductivity of ITO layers reached 130–140 S cm^{-1} after annealing in hydrogen at a relatively low temperature of 250 °C or 300 °C.[19,20] However, the release of gas during the combustion of precursors limits this method mostly to very thin or/and amorphous layers.

Metal hydroxides are less explored precursors in the fabrication of conductive TCO layers, although the hydroxide precursor has been used in the synthesis of metal oxide nanocrystals, such as TiO_2,[21] In_2O_3 (ref. 22) and ITO.[23] The phase transformation from metal hydroxide to oxide only involves a step of water condensation. In the case of undoped In_2O_3, the hydroxide phase can be transformed into the crystalline oxide at a mild temperature of 200–300 °C.[24,25]

In this work, we explore the low temperature crystallization of conductive ITO layers based on inks composed of indium tin hydroxide (ITOH) nanoparticles. Surface modification with ethanolamine (ETA) molecules can reduce the phase transformation temperature to *ca.* 250 °C and promote crystallization into the bixbyite ITO phase. The assistance of ETA treatment in speeding up the dehydration of hydroxide, promoting the earlier crystallization as well as increase of crystal size after the same annealing is investigated with several complementary methods. An improved electrical conductivity of 43 S cm^{-1} combined with a high optical transmittance above 90% is demonstrated for nanoparticle-processed ITO layers annealed at 300 °C.

2. Experimental

2.1 Sample preparation

Nanoparticle derived layers were fabricated *via* the spin coating of hydroxide nanoparticle inks. The sample preparation included four steps: (1) solvent thermal synthesis of nanoparticles and ink preparation, (2) spin-coating of nanoparticle ink in an NH_3-containing atmosphere, (3) ETA modification of NP derived layers and (4) post-annealing of NP derived layers (with and without ETA modification) in forming gas (95% N_2/5% H_2) at 300 °C. A sequential order of the four steps is illustrated in Fig. 1.

Step (1): preparation of additive-free nanoparticle ink. The synthetic method of nanoparticles was modified from a previous publication.[26] Indium tri-chloride ($InCl_3$, Sigma-Aldrich, 98%) and tin tetra-chloride ($SnCl_4$, Sigma-Aldrich, nonaqueous, 98%) were taken as metal precursors, while solid NaOH (granule, Sigma-Aldrich) as the catalyst and ethylene

Fig. 1 Preparation procedure for nanoparticle derived layers with ETA modification.

glycol (Carl Roth, 99%) as the solvent. All the chemicals were used without further treatment. The molar ratio between $InCl_3$ and $SnCl_4$ was maintained as 9 : 1 (10% doping), and a reaction temperature of 190 °C and a reaction time of 6 days were selected for the synthesis. The reacted nanoparticles were collected *via* centrifugation at 12 000 rpm min^{-1} for 15 min (Eppendorf, Centrifuge 5810R), and the collected nanoparticles were washed twice with distilled water to remove solvent residuals. To prepare nanoparticle ink, the collected nanoparticles (without drying) were re-dispersed in distilled water (DI) under magnetic stirring, without adding any stabilizing agents or organic additives. A series of inks with different solid loadings (concentrations) ranging from 2 wt% to 30 wt% could be prepared by adding the required amount of distilled water into the collected nanoparticles. The prepared inks are visually clear and free of sedimentation even after over 1 year storage at room temperature.

Step (2): spin coating under a controlled atmosphere. Spin-coating was performed at room temperature, with a rotation speed of 2000 rpm min^{-1} and a duration of 30 seconds for each layer. Soda-lime glasses, with a thickness of 1 mm and a size of 2.5 × 2.5 cm, were taken as substrates for depositing the prepared nanoparticle inks. They were cleaned in a consequential order with diluted acetic acid, isopropanol and DI water, and finished with oxygen plasma cleaning for 5 min to improve surface wettability. In order to achieve nanoparticle layers free of cracks and surface defects, ink concentration as well as the chamber atmosphere was optimized.

To minimize the presence of cracks in the obtained nanoparticle layer, ink concentrations varying from 30 wt% to 2 wt% were tested in a manner of single layer. With the optimized ink concentration (2 wt%), the spin-coating process was repeated multiple times to obtain the required thickness and a heating step at 80 °C for 1 min was applied between every two adjacent layers. The NH_3-containing chamber atmosphere was found effective in reducing surface defects such as streaks and comets and improving layer homogeneity. This atmosphere was generated by spin-coating 14 wt% NH_4OH water solution on a spare substrate, which was different from the substrates used for the spin-coating of nanoparticle layers. Afterwards, the spare substrate was taken out of the spin-coating chamber and the atmosphere was generated, followed by the fabrication of nanoparticle layers.

Step (3): ETA modification of nanoparticle derived layers. Ligand modification was performed on the as-deposited precursor layers before the final annealing step. Ethanolamine (ETA, Sigma-Aldrich, ≥98%) was selected for ligand modification of hydroxide precursor layers. ETA was first dissolved in absolute ethanol with a concentration of 5 mM, and the samples were fixed in a Teflon sample holder and immersed in the solution for 24 hours. The solution was stirred at room temperature during the immersion time. The samples were rinsed with isopropanol continuously for 3 min after taking out from the ETA solution. We also attempted direct mixing of ligands into the nanoparticle ink; however, it caused
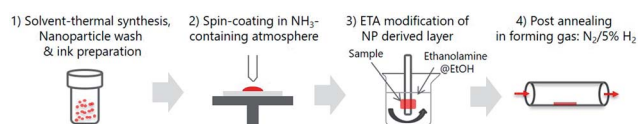
3084 | *J. Mater. Chem. A*, 2019, 7, 3083–3089

This journal is © The Royal Society of Chemistry 2019

agglomeration of nanoparticles and the spin-coated layers showed a much rougher surface.

Step (4): post annealing in forming gas. Nanoparticle layers with and without ETA modification were dried for 30 min on a preheated hot plate in air and then annealed for 3 hours in forming gas (mixture of 95% N_2 and 5% H_2) at 300 °C.

2.2 Characterization techniques

ITOH nanoparticle dispersions were characterized by dynamic light scattering (DLS) and zeta potential on a Zetasizer Nano series (Malvern). High resolution transmission electron microscopy (HRTEM) was performed using a field emission FET Titan 80-300 operated at 300 kV. Thermal gravimetric analysis (TGA) and differential scanning calorimetry (DSC) on nano-particle powder were performed with a Netzsch STA 449 F3 Jupiter in synthetic air in a temperature range from room temperature to 600 °C at a ramping speed of 5 °C per min.

Thin layers before and after annealing were analysed by X-ray photoelectron spectroscopy (XPS) measurements on a Quantum 2000 from Physical Electronics with a monochromatic Al Kα source (1486.6 eV) operated at a base pressure below 8×10^{-7} Pa. X-ray diffraction (XRD) analysis of nanoparticle layers was carried out to detect the phase transformation of nanoparticle layers with and without ETA modification along with the increase of annealing temperatures. The measurements were performed on a PANanalytical diffractometer (X'Pert Pro PW3040) equipped with Ni-filtered Cu Kα-radiation ($\lambda = 1.5406$ Å). *In situ* XRD measurements were conducted at temperatures of 200 °C, 225 °C, 250 °C, 275 °C and 300 °C, with a holding time of 30 min at each temperature. Transmittance was measured with a UV-Vis spectrometer Shimadzu UV-3600 from 200 nm to 2000 nm taking air as the reference (baseline). The electrical dc conductivity of annealed layers was measured by Hall-effect measurement on ECOPIA HMS3000 apparatus using the van der Pauw contacting configuration with gold contacts.

3. Results and discussion

3.1 Fabrication and characterization of ITOH nanoparticles and ITOH layers

The ITOH nanoparticles synthesized by this solvent-thermal approach at 190 °C exhibit a hexagonal structure, different from the cubic phase of bixbyite ITO.[26] ITOH nanoparticles can be transferred into the crystalline cubic ITO phase at a mild temperature of 300 °C (in the form of dry powder), enabling their use as precursors or building blocks for various nano-structures of ITO electrodes.[26] Another feature of such nano-particles is their facile dispersibility in water, which facilitates the formation of water-based nanoparticle inks with long-term stability even at high solid loadings up to 30 wt% as tested in this work.

In Fig. 2, high resolution TEM images reveal the size of single nanoparticles as *ca.* 5 nm, near spherical in shape, and crys-talline in phase as visible from lattice fringes. Measurements with DLS show that the particles re-dispersed in DI-water are slightly agglomerated, with the peak of the distribution at 15–
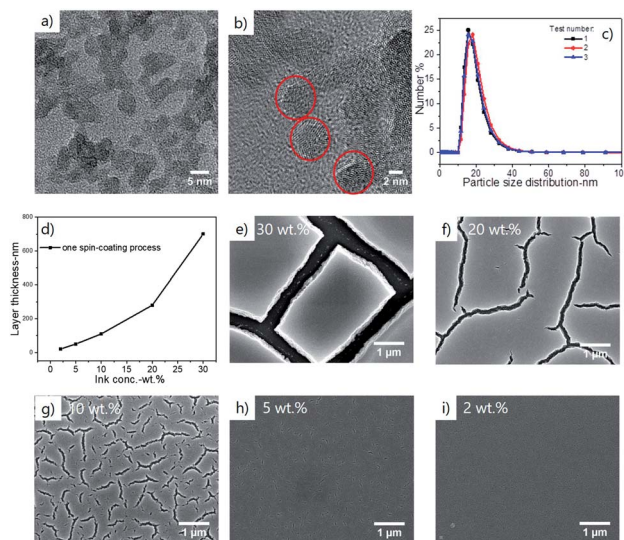

Fig. 2 (a and b) TEM morphology and (c) size distribution of solvent-thermal synthesized indium tin hydroxide nanoparticles re-dispersed in DI water (DLS); (d) the correlation between layer thickness and ink concentration; SEM top-views of spin-coated nanoparticle layers from (e) 30 wt% ink, (f) 20 wt%, (g) 10 wt%, (h) 5 wt% and (i) 2 wt%.

16 nm (Fig. 2c), indicating that the particles exist in clusters. The dispersion exhibits a zeta-potential of +39 mV and is very stable. The positive character of zeta potential is due to its adsorbed positively charged protons to counter near surface hydroxyl groups. No sedimentation is observed even after one-year storage in a closed vial at room temperature. No addi-tives or stabilizing agents were further added into the ink of indium tin hydroxide nanoparticles.

The thickness of one step spin-coated layer correlates with the ink concentration, as shown in Fig. 2d. Although a solid loading as high as 30 wt% can be achieved without stabilizing agents, the occurrence of cracks in fabricated nanoparticle layers was almost inevitable for inks with a high concentration (see Fig. 2e–i). To limit the crack formation, the ink concen-tration was decreased to 2 wt% and the thickness of a single spin-coating obtained layer was *ca.* 20 nm. Therefore, a multiple spin-coating process was performed in order to achieve a nanoparticle layer with required thickness.

Besides the effect of ink concentration on the quality of coated layers, it was found out that the coating atmosphere also plays an important role, especially in avoiding the generation of surface defects such as 'streaks' and 'comets'. As reported by Redel[27] and Puzzo,[28] streaks and comets are frequent defects in spin-coated nanoparticle layers because of particle agglomera-tion, dust particles in air, inappropriate setting of spin-coating parameters, *etc.* Our coating practice indicates that such defects can be avoided by generating a suitable atmosphere within the spin-coater chamber. In our case, an NH_3-containing atmo-sphere has helped to reduce the number of defects such as comets/streaks and improve film homogeneity. The role of the NH_3-containing atmosphere could be related to the surface characteristics of our hydroxide nanoparticles, which possess a positive zeta-potential of +39 mV, indicating the existence of

a positively charged surface double-layer. The spin-coating of a layer of NH₄OH solution in the spin-coating chamber provided NH₄⁺ cations to the environment, and these cations could adsorb to the nanoparticle surface and further increase the surface charge of these nanoparticles. Consequentially, the nanoparticles were better stabilized and the number of surface defects due to nanoparticle agglomeration during the spin-coating process was clearly reduced.

3.2 The effect of ETA modification on the phase transformation of hydroxide into ITO

We selected to conduct ETA modification on spin-coated precursor layers instead of mixing the solution of ETA with the ITOH nanoparticle ink. The reason behind this is that the addition of ETA into the nanoparticle ink inevitably caused the agglomeration of nanoparticles. The dispersion of ITOH nanoparticles shows a zeta-potential of +39 mV and the double layer of nanoparticles is positively charged due to adsorbed protons. Adding ETA (a Lewis base) into the nanoparticle ink can reverse the characteristics of the nanoparticle double layer and induce their agglomeration.

The effect of ETA modification is first revealed by the differences in oxygen 1s peaks of XPS measurement. As shown in Fig. 3a–d, the oxygen 1s peaks can be de-convoluted into two separate peaks: peak 1 is positioned at ~530.0–530.5 eV and corresponds to the metal–oxygen bonding, while peak 2 is positioned at ~531.5–531.8 eV and corresponds to the hydroxyl groups. The fitting results for non-treated and ETA-modified samples indicate that the area ratio of peak 2 increased from 42% to 55% for samples before the annealing, while it decreased from 25% to 15% for samples after the annealing. Apparently, the ETA modification has affected the phase transformation in two aspects: (1) it promoted a further

hydrolysis based on hydroxide nanoparticles before the annealing process (2) and resulted in a higher level of condensation or dehydration after the annealing process at 300 °C, leading to a decreased number of hydroxyl groups.

It was also noticed that the loss of hydroxyl groups due to condensation or dehydration during the annealing process becomes quicker as compared to the non-treated sample. As shown in the DSC measurement in Fig. 4a and b, coupled with a higher exothermic peak, the weight loss at around 250 °C has a sharper slope comparing with the non-treated sample, indicating a faster removal of hydroxyl groups; consequently, completion of the phase transformation from hydroxide to oxide (step (3)) is shifted to a lower temperature. Besides, the amount of weight loss of steps (2) and (3) was also higher than that of the non-treated sample, with 18.1% against 17.0% (9.5% + 7.5%), which implies that the sample with ETA modification possesses a larger number of hydroxyl groups before annealing, as already detected by XPS. After the completion of the phase transformation, the number of residual surface hydroxyl groups (indicated by step (4)) is lower for the ETA-treated sample, which is in agreement with XPS results. The sharp exothermal peak at 400 °C stems from the oxidation of the ETA residues which could be trapped by the nanoparticle powder after soaking in the ETA–ethanol solution (autoignition temperature of ETA is 410 °C). The ETA residues are not present in 300 nm-thin ITOH layers because no traces of amino-groups were detected by XPS (not shown).

The shift of phase transformation to a lower temperature is also confirmed with *in situ* XRD measurement, shown as an earlier onset/appearance of the crystalline ITO phase under the same annealing conditions (Fig. 4c and d). Several studies on the phase transformation of indium hydroxide powder into the oxide phase reported the re-dissolution of indium hydroxide into an amorphous phase at 200–250 °C and the generation of a crystalline oxide phase from a re-nucleation process.[23,26] In our case, no transformation of hydroxide into an amorphous phase
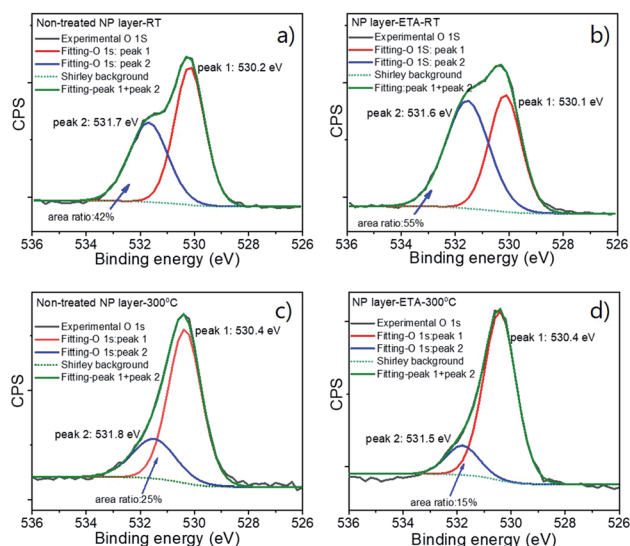

Fig. 3 XPS O 1s peak of nanoparticle derived layers (a) and (b) before annealing, (c) and (d) after annealing with and without ethanolamine modification.
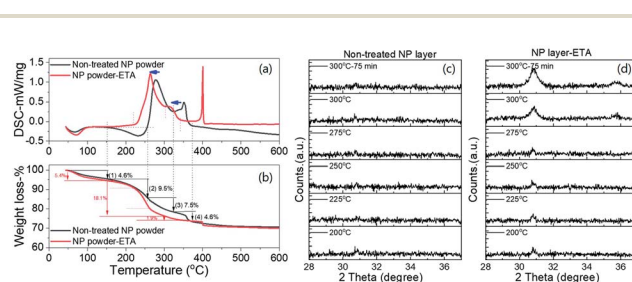

Fig. 4 Thermal analysis and *in situ* XRD measurement of non-annealed nanoparticle samples with and without ETA modification. The DSC/TG profiles in (a) and (b) show the transformation process, which can be divided into four steps: (1) evaporation of moisture before 150 °C, shown as a weight loss of 4.6% and 5.4% for the non-treated sample and ETA modified sample; (2) the removal of hydrated water (adsorbed molecular water) and (3) phase transformation from hydroxide to oxide, which in total counts for 17.0% loss for the non-treated sample and 18.1% loss for the ETA modified sample; (4) removal of surface hydroxyl groups at higher temperatures, accounting for 4.6% for the non-treated sample and 1.9% for the ETA modified sample. The *in situ* XRD patterns of the (c) as-deposited non-treated NP layer and (d) ETA modified layer.

was detected. We do not know whether this is because of the layer thickness restriction or from the ETA modification.

Amines have been reported to assist in the synthesis of metal oxides by complexing with metal ions and hindering their fast hydrolysis, *i.e.* acting as stabilizing ligands.[23,29] In the present case, the ETA acts in a different way by speeding up the condensation/dehydration and inducing an earlier crystallization of the hydroxide ITOH precursor into the ITO phase. One hypothesis is that the surface of hydroxide nanoparticles gets functionalized with amino-containing ligands, which can be oxidized upon subsequent annealing in air. Through this exothermic reaction, energy is provided to hydroxide precursors (in a so-called combustion synthesis[19,30]). Such a hypothesis of the combustion synthesis is supported by the stronger exothermal peak of the ETA-modified sample (Fig. 4a). However, no traces of amino-groups could be detected in the full spectrum XPS of non-annealed layers (not shown), so this effect cannot be dominant. A second mechanism could be related to the hydroxyl groups from ethanolamine molecules, which further promoted the hydrolysis of our as-prepared nanoparticle layers, seen as an increased number of hydroxyl groups compared with the reference sample in Fig. 3a and b, and finally resulted in a faster and higher level of dehydration/condensation and earlier onset of crystallization. This effect has been reported in a recent work by Jao and others.[31] With the presence of hydroxyl anions from tetramethylammonium hydroxide (TMAOH), the reaction rate for synthesizing NiO from nickel acetate was increased by two times, while the activation energy was decreased from 107 kJ mol^{-1} to 59 kJ mol^{-1}.

3.3 The effect of ETA modification on the conductive properties of nanoparticle ITO layers

It can be expected that the ETA-modified nanoparticle layer exhibits a higher crystallinity and larger crystal size after annealing as compared to the non-treated layer. This is evidenced by XRD patterns in Fig. 5a. The grain size (or more precisely the crystal coherence length) calculated using the Debye–Scherrer formula from the full-width-at-half-maximum of (222), (400) and (440) reflexes is 35.3 nm, 34.3 nm, and 31.9 nm, which is larger than 30.5 nm, 29.4 nm, and 28.7 nm for the non-treated sample. The top-view SEM images also reflect the difference of crystal sizes, as shown in Fig. 5b. The larger voids that appear in the top view SEM image of the ETA modified layers might be a consequence of crystal growth. ETA
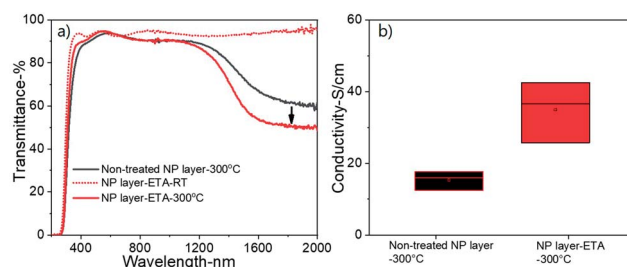

Fig. 6 (a) UV-Vis transmittance spectra and (b) dc conductivity of nanoparticle derived layers with and without ETA modification.

modification has no effect on the layer thickness, which is 310 ± 10 nm for both samples.

The obtained ITO layers are transparent in the visible wavelength range, with a transmittance above 90% in the 380–1100 nm wavelength range (Fig. 6a). In the IR range after 1100 nm the free carrier-induced IR absorption starts to appear and it is more pronounced for the ETA-modified layer. The difference in free carrier concentration can be explained by the different number of surface hydroxyl groups after the annealing process as measured by XPS. As proposed by Heiland and Morrison,[32,33] the adsorbed oxygen species such as hydroxyl groups or hydrated water trap electrons from the surface region of n-type metal oxide particles and form a depletion layer. The existence of the depletion layer hinders the electron transport across the grain boundaries and also reduces carrier concentration. The experimental correlation between the presence of adsorbed surface states and the electrical conductive properties of nanoparticle-derived TCO layers has also been reported in recent studies from the Milliron group.[8,34] In our case, a reduced number of surface hydroxyl groups correlate with a higher concentration of charge carriers, which also induces a shift of the UV cut-off to a shorter wavelength (the Burstein–Moss shift).

Electrical conductivity, a parameter correlated with layer crystallinity and charge carrier concentration, reflects the effect of ETA modification on the nanoparticle ITO layer. As plotted in Fig. 6b, the measured dc conductivities of ETA modified layers are two times higher than those of the non-treated layers. A high conductivity of 43 S cm^{-1} (sheet resistance of 782 Ω sq^{-1}) has been measured for ETA modified layers annealed at 300 °C in forming gas of 5% H_2/N_2. Compared with references,[7,19] this is not the highest value for solution processed TCOs at a temperature of 300 °C. However, an optimization of the modification process still holds potential for further reducing the crystallization temperature of the ITO phase and improvement of electrical properties.

4. Conclusions

Taking ITOH as a precursor, the fabrication of nanoparticle layers *via* multiple spin-coating of a stable additive-free hydroxide ink is demonstrated. Surface modification with ETA on a spin-coated nanoparticle layer can promote the phase transformation of hydroxide into the crystalline ITO phase, which results in an earlier onset of crystallization and larger
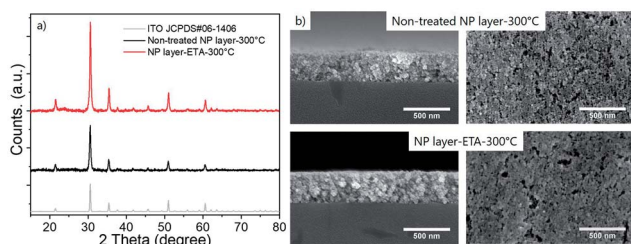

Fig. 5 (a) XRD and (b) SEM images of nanoparticle derived layers with and without ETA modification after the annealing process at 300 °C.

crystal size after the same annealing. The ETA modification also results in fewer hydroxyl groups after the annealing process, thus yielding a higher charge carrier concentration and dc conductivity two times higher than that of the non-treated layer. A conductivity of 43 S cm^{-1} combined with an optical transmittance above 90% is demonstrated for an ITO layer processed from a dispersion of hydroxide nanoparticles.

Conflicts of interest

There are no conflicts to declare.

Acknowledgements

References

1 B. G. Lewis and D. C. Paine, Applications and Processing of Transparent Conducting Oxides, *MRS Bull.*, 2011, **25**(8), 22–27.

2 K. Ellmer, Past achievements and future challenges in the development of optically transparent electrodes, *Nat. Photonics*, 2012, **6**, 809.

3 D. S. Ginley and C. Bright, Transparent Conducting Oxides, *MRS Bull.*, 2011, **25**(8), 15–18.

4 R. M. Pasquarelli, D. S. Ginley and R. O'Hayre, Solution processing of transparent conductors: from flask to film, *Chem. Soc. Rev.*, 2011, **40**(11), 5406–5441.

5 J. Perelaer, *et al.*, Printed electronics: the challenges involved in printing devices, interconnects, and contacts based on inorganic materials, *J. Mater. Chem.*, 2010, **20**(39), 8446–8453.

6 R. W. Schwartz, T. Schneller and R. Waser, Chemical solution deposition of electronic oxide films, *C. R. Chim.*, 2004, **7**(5), 433–461.

7 J. Song, *et al.*, Back Cover: A General One-Pot Strategy for the Synthesis of High-Performance Transparent-Conducting-Oxide Nanocrystal Inks for All-Solution-Processed Devices, *Angew. Chem., Int. Ed.*, 2015, **54**(2), 698.

8 J. Ephraim, *et al.*, Transparent Conductive Oxide Nanocrystals Coated with Insulators by Atomic Layer Deposition, *Chem. Mater.*, 2016, **28**(15), 5549–5553.

9 J.-Y. Kim and N. A. Kotov, Charge Transport Dilemma of Solution-Processed Nanomaterials, *Chem. Mater.*, 2014, **26**(1), 134–152.

10 J. Ederth, *et al.*, Indium tin oxide films made from nanoparticles: models for the optical and electrical properties, *Thin Solid Films*, 2003, **445**(2), 199–206.

11 J. Ederth, *et al.*, Electrical and optical properties of thin films consisting of tin-doped indium oxide nanoparticles, *Phys. Rev. B: Condens. Matter Mater. Phys.*, 2003, **68**(15), 155410.

12 J. Ba, *et al.*, Crystallization of indium tin oxide nanoparticles: from cooperative behavior to individuality, *Small*, 2007, **3**(2), 310–317.

13 D. Ito, *et al.*, Synthesis of Ligand-Stabilized Metal Oxide Nanocrystals and Epitaxial Core/Shell Nanocrystals *via* a Lower-Temperature Esterification Process, *ACS Nano*, 2014, **8**(1), 64–75.

14 B. H. Kim, *et al.*, High Mobility in Nanocrystal-Based Transparent Conducting Oxide Thin Films, *ACS Nano*, 2018, **12**(4), 3200–3208.

15 M. Toshiro and K. Akira, Indium-Tin Oxide Thin Films Prepared by Thermal Decomposition of Metallic Complex Salts, *Jpn. J. Appl. Phys., Part 2*, 1988, **27**(10A), L1829.

16 S. Seki, *et al.*, Highly conducting indium-tin-oxide transparent films prepared by dip-coating with an indium carboxylate salt, *Surf. Coat. Technol.*, 2003, **169–170**, 525–527.

17 R. B. H. Tahar, *et al.*, Electronic transport in tin-doped indium oxide thin films prepared by sol-gel technique, *J. Appl. Phys.*, 1998, **83**(4), 2139–2141.

18 I. Bretos, *et al.*, Low-temperature crystallization of solution-derived metal oxide thin films assisted by chemical processes, *Chem. Soc. Rev.*, 2018, **47**(2), 291–308.

19 M.-G. Kim, *et al.*, Low-temperature fabrication of high-performance metal oxide thin-film electronics *via* combustion processing, *Nat. Mater.*, 2011, **10**, 382.

20 X. Yu, *et al.*, Spray-combustion synthesis: Efficient solution route to high-performance oxide transistors, *Proc. Natl. Acad. Sci. U. S. A.*, 2015, **112**(11), 3217–3222.

21 J.-N. Nian, *et al.*, Structural Feature and Catalytic Performance of Cu Species Distributed over TiO$_2$ Nanotubes, *J. Phys. Chem. B*, 2006, **110**(51), 25817–25824.

22 S. Tang, *et al.*, Effects of Heating Rate on the Nucleation, Growth, and Transformation of InOOH and In$_2$O$_3$ *via* Solvothermal Reactions, *J. Phys. Chem. C*, 2014, **118**(36), 21170–21176.

23 Z. Chen, *et al.*, Ethanolamine-assisted synthesis of size-controlled indium tin oxide nanoinks for low temperature solution deposited transparent conductive films, *J. Mater. Chem. C*, 2015, **3**(43), 11464–11470.

24 X. Xu and X. Wang, Size- and Surface-Determined Transformations: From Ultrathin InOOH Nanowires to Uniform c-In$_2$O$_3$ Nanocubes and rh-In$_2$O$_3$ Nanowires, *Inorg. Chem.*, 2009, **48**(8), 3890–3895.

25 L. A. Pérez-Maqueda, L. Wang and E. Matijević, Nanosize Indium Hydroxide by Peptization of Colloidal Precipitates, *Langmuir*, 1998, **14**(16), 4397–4401.

26 Y. Liu, *et al.*, Assembly of mesoporous indium tin oxide electrodes from nano-hydroxide building blocks, *Chem. Sci.*, 2012, **3**(7), 2367–2374.

27 E. Redel, *et al.*, Hierarchical Nanoparticle Bragg Mirrors: Tandem and Gradient Architectures, *Small*, 2011, **7**(24), 3465–3471.

28 D. P. Puzzo, *et al.*, Color from colorless nanomaterials: Bragg reflectors made of nanoparticles, *J. Mater. Chem.*, 2009, **19**(21), 3500–3506.

29 L. Znaidi, *et al.*, Oriented ZnO thin films synthesis by sol–gel process for laser application, *Thin Solid Films*, 2003, **428**(1), 257–262.

30 N. Martin-Arbella, *et al.*, Photoactivation of Sol-Gel Precursors for the Low-Temperature Preparation of PbTiO$_3$

3088 | *J. Mater. Chem. A*, 2019, **7**, 3083–3089

This journal is © The Royal Society of Chemistry 2019

Ferroelectric Thin Films, *J. Am. Ceram. Soc.*, 2011, **94**(2), 396–403.

31 M. Jao, Low temperature and rapic formation of high quality metal oxide thin film *via* a hydroxide-assisted energy conservation strategy, *J. Mater. Chem. C*, 2018, **6**, 9941–9949.

32 S. R. Morrison, Surface Barrier Effects in Adsorption, Illustrated by Zinc Oxide, in *Advances in Catalysis*, ed. W. G. Frankenburg, V. I. Komarewsky and E. K. Rideal, Academic Press, 1955, pp. 259–301.

33 G. Heiland, E. Mollwo, and F. Stöckmann, Electronic Processes in Zinc Oxide, in *Solid State Physics*, ed. F. Seitz and D. Turnbull, Academic Press, 1959, pp. 191–323.

34 C. M. Staller, *et al.*, Tuning Nanocrystal Surface Depletion by Controlling Dopant Distribution as a Route Toward Enhanced Film Conductivity, *Nano Lett.*, 2018, **18**(5), 2870–2878.